Spectrochimica Acta Part A: Molecular and Biomolecular Spectroscopy 202 (2018) 376–381

Contents lists available at ScienceDirect

Spectrochimica Acta Part A: Molecular and Biomolecular Spectroscopy

journal homepage: www.elsevier.com/locate/saa

Rapid fabrication of flexible and transparent gold nanorods/poly (methyl methacrylate) membrane substrate for SERS nanosensor application

Nan Yang, Ting-Ting You, Yu-Kun Gao, Chen-Meng Zhang, Peng-Gang Yin *

Beihang University, School of Chemistry, Key Laboratory of Bio-Inspired Smart Interfacial Science and Technology of Ministry of Education, Beijing 100191, China

ARTICLE INFO

Article history:
Received 9 March 2018
Received in revised form 15 May 2018
Accepted 16 May 2018
Available online 17 May 2018

Keywords:
Au nanorods
Surface-enhanced Raman scattering
Flexible membrane
Plasmonic nanosensor
Finite-difference time-domain

ABSTRACT

Flexible substrates have been proposed for daily-life applications in SERS detection due to the prominent sample collection properties such as they can be wrapped around non-planar object surface. Combining the noble metals with polymers, flexible SERS substrates could be fabricated with advantages of light weight, transparency and high SERS sensitivity. Herein, we prepare a gold nanorods (AuNRs)/poly(methyl methacrylate) (PMMA) film as flexible SERS substrate by self-assembling a uniformly AuNRs array layer on PMMA template. This AuNRs/PMMA film performs excellently on thiram trace detection with the lowest detection concentration of 0.5 ppb. The fabricated substrates were applied for practical detection with cucumber by directly covering the AuNRs/PMMA flexible film on the target surface. Furthermore, the high SERS sensitivity as well as great reproducibility present a wide range of prospections for the further application of non-plane surface.

1. Introduction

Surface-enhanced Raman scattering (SERS) has been developed in analytical sciences, biological sciences, surface and material sciences due to its nondestructive analysis and ultrasensitive properties [1–4]. Extensive efforts have focused on the exploration of the SERS mechanisms and there are two major enhancement mechanisms have been widely accepted, electromagnetic enhancement and chemical enhancement. [5,6] The electromagnetic enhancement defined the interaction between the incident and scattered light and substrate which arise intense field enhancement factor due to the excitation of localized surface plasmon resonance (LSPR) of the nanoparticle metal surface. The chemical enhancement produced by exceting of adsorbed molecules localized electronic resonances or the chemical interaction between the adsorbed probes and the adsorptive surface [7]. The "SERS hot spots" are small gaps between nanoparticles, and the coupling effect between nanoparticles generally accepted as the regions of highly enhanced local electromagnetic field which is the dominant contribution for SERS enhancement [6,8]. In this field, metallic nanoparticles suspensions were widely used because of the high SERS performance [9]. However, the reproducibility of the substrate restricted the broad application until the problem was solved by immobilizing the metallic nanoparticles on certain kind of solid support such as glass, quartz and silicon substrates [10]. So far, great efforts have been focused on non-flexible substrates to realize high SERS activity and reproducibility by methods as the Langmuir–Blodgett (LB) method, the template method, and nanolithography and nanoimprint methods [11,12]. However, disadvantages exist such as brittle, nonflexible and inconvenient in practical application. In comparison, it is more easy and efficiently to collect spectral signal via flexible substrates, which could achieve broader application and meet varied realistic demands [13].

Over the past few years, a number of flexible SERS substrates have been obtained by means of nanofiber assemblies, cellulose paper, carbon nanotube (CNT) or grapheme templates and oblique angle deposition (OAD) technique [14–18]. However, those flexible SERS materials reported in literature exist some inherent problems such as poor optical transparency, complicated preparation process, harsh reaction conditions and high fabrication costs. Taking the above shortcomings into account, fabricating flexible SERS substrates on plastic or polymers can offer advantages of light weight, transparency, efficient fabrication and low cost based on the flexible properties [19–21]. It is important to note that metal-polymer flexible SERS substrates pay attention to high and uniform SERS signal enhancement as well as excellent transparency and flexibility. Noble metals such as Ag, Au, Cu are commonly used as SERS substrates due to the high electromagnetic enhancement [22]. Compared with the sphere-shape nanoparticles, gold nanorods (AuNRs), as an anisotropic nanostructure, have stronger electromagnetic enhancement capacity on account of the lightning rod effect [23]. AuNRs display two separate surface plasmon resonance (SPR) bands known as transverse and longitudinal plasmon bands [24]. The peaks are tunable depending on the aspect ratio of the AuNRs, this

* Corresponding author.
E-mail address: pgyin@buaa.edu.cn (P.-G. Yin).

https://doi.org/10.1016/j.saa.2018.05.068
1386-1425/

characteristic broadens their application in biotechnologies by manipulating the longitudinal band in the nearinfrared (NIR) region [25].

Herein, we report a facile and practicable method for fabricating the AuNRs/PMMA film served as a flexible SERS substrate via self-assemble of AuNRs in poly(methyl methacrylate) (PMMA) template. AuNRs located uniformly in one side of the film, which can contribute spectral enhancement and intensive hotspots. The other side of AuNRs/PMMA film (PMMA template layer) is optically transparent, so the laser can easily pass through PMMA template and reach the assembled AuNRs layer which means we can use AuNRs layer to connect with analytes and obtain Raman signal from the side of PMMA. It is worth mentioning that the minimum detectable concentration for thiram detection on the previous preparation substrate can be as low as 0.5 ppb. Furthermore, we can obtain clear Raman signals for the trace-detection by covering the AuNRs/PMMA flexible film directly on the surface of cucumber sample, indicating that this as-synthesized flexible SERS substrate is suitable for diverse morphologies surface. Therefore, the AuNRs/PMMA flexible film can provide a practical SERS active platform for the trace analysis with cost-effective, high reproducibility, sensitivity and stability.

2. Materials and Methods

2.1. Reagents

Chloroauric acid ($HAuCl_4$) and Poly(methyl methacrylate) (PMMA, MW = 1.2×10^5 g/mol) used for this study were purchased from Sigma Aldrich (Shanghai, China). P-mercaptobenzoic acid (p-MBA) were purchased from Tokyo chemical industry Co. Cetyltrimethyl Ammonium Bromide (CTAB) were purchased from Lanyi Factory Co. (Beijing, China). Sodium oleate (NaOL) were purchased from Hushi laborator equipment Co. (Shanghai, China). Silver nitrate ($AgNO_3$) and sodium borohydride ($NaBH_4$) were purchased from Guanghua Chemical Factory Co. (Guangdong, China). Ascorbic acid (AA) were purchased from Xilong Factory Co. (Guangdong, China). All syntheses progresses were used Ultrapure MilliQ water. All the glassware was soaked in aqua regia following which the substrates were rinsed with MilliQ water for several times and then dried before use.

2.2. Synthesis of the AuNRs

Seeds mediated growth method is adopted to synthesize monodisperse AuNRs with high aspect ratio [26].

2.2.1. Synthesis of the Seed of Gold Nanorods

First 5 mL $HAuCl_4$ solution (0.5 mM) and 5 mL CTAB (0.2 M) solution are mixed in a 100 mL boiling flask. Additional 0.6 mL fresh ice $NaBH_4$ (0.01 M) is diluted to 1 mL with pure water and then injected to the previous mixed solutions under vigorous stirring (1200 rpm). Keep stirring for 2 min until the color of the seed solutions change to brownish yellow. Stop stirring and keep the solutions stewing at least 30 min before use at room temperature to complete the reaction.

2.2.2. Preparation of the Growth Solution

3.5 g CTAB and 0.617 g NaOL were dissolved by pure water approximately at 50 °C in a 250 mL flask. Then 9 mL $AgNO_3$ solution (4 mM) was added when previous solution was cool down to 30 °C. Keep this solution undisturbed at 30 °C for 15 min before the additional 125 mL $HAuCl_4$ solution (1 mM) was added. After 90 min of stirring (700 rpm) the solution became colorless, following 0.75 mL HCl was added to adjust the pH. Then slow stirring 15 min at 400 rpm and changed to vigorous stirring at 1200 rpm after added 0.625 mL ascorbic acid (0.064 M), and stirred another 30 s at 1200 rpm after 0.2 mL gold seed solution was added. Finally, keep the mixed solution undisturbed at 30 °C at least 12 h for fully growth of AuNR. Centrifuge the final products at 7000 rpm for 20 min and remove the supernatant, repeat this procedure three times. It's better to use warm water to wash CTAB out. Isochoric the AuNRs at 10 mL.

2.3. Fabrication of Gold Nanorods/PMMA Flexible Substrates

First, dilute 0.3 mL prepared AuNRs suspension to 1.5 mL with MilliQ water (about 2 nM), and transferred diluted AuNRs to a beaker. Then insert the syringe needle with ethanol to the solution before add 0.7 mL toluene with 26 mg PMMA to beaker. There was a clear water/toluene interface formed as soon as toluene was added, which caused by incompatibility of two liquid. After that, the peristaltic pump was used to injected 0.8 mL ethanol with the feeding rate of 0.12 mL/min. It is noteworthy that a same liquid volume between AuNRs suspension and ethanol together with toluene was crucial. The AuNRs were slightly rose up to the water/toluene interface and spontaneously self-assembled into an array monolayer with a thin PMMA film along with the evaporation of toluene. While the toluene volatile completely, a flexible transparent PE film was used as a support to retrieve the AuNRs/PMMA film, and subsequently dried at 60 °C temperature.

2.4. Fabrication of SERS Sample

For the SERS sensitivity measurement, small pieces of the AuNRs/PMMA film were immersed in 0.2 mL of 10^{-3} M p-MBA solution for 4 h, then taken out and dried in air. To determine SERS enhancement factor, the sample was immersed in 10^{-9} M CV solution for 4 h, then taken out washed with ethanol to remove the unbound molecules and dried in air. For thiram detection, a series of standard thiram solutions of different concentrations (from 5 ppm to 0.5 ppb) were prepared by diluting the stock solution with water, then immersed film substrates in 0.2 mL thiram solution for 4 h, then taken out and dried in air. For

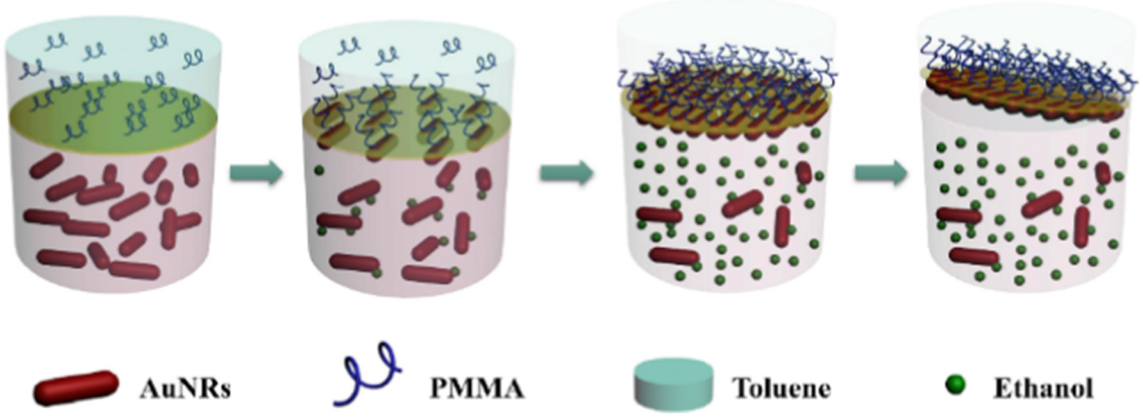

Scheme 1. Schematic diagram of preparation of AuNRs/PMMA SERS substrate.

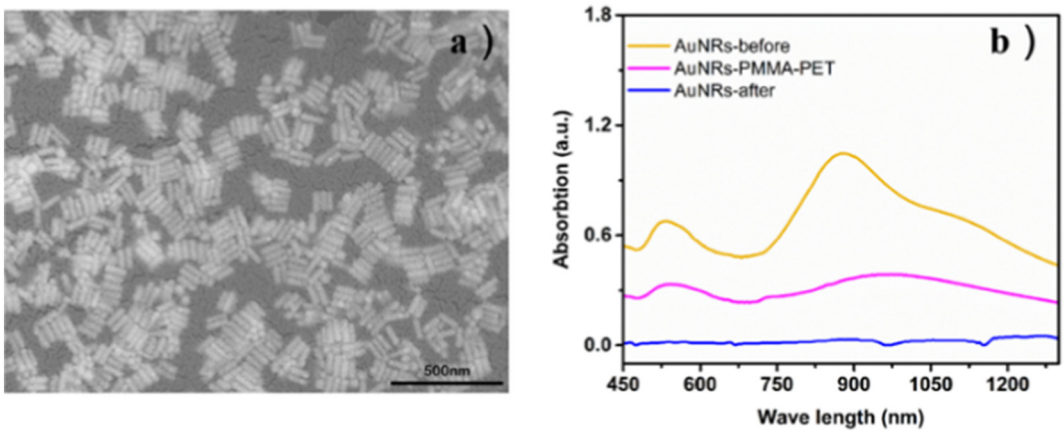

Fig. 1. (a) The SEM image of the AuNRs/PMMA film; (b) UV–vis spectra of monodispersed AuNRs solution, AuNRs-PMMA film supported by PET and AuNRs solution after assembly.

pesticide detection on vegetable skin, pieces of cucumber were first soaked in thiram solutions with different concentrations (from 5 ppm to 50 ppb), followed by covering a AuNRs/PMMA film around the skin, with the AuNRs facing it.

2.5. Characterization

Field emission scanning electron microscopy (FE-SEM) was performed on a Jeol-JSM 7500 scanning electron microscope (SEM) with an accelerating voltage of 3.0 kV. The UV–vis spectrophotometer and fittings were provided by SHIMADZU (Japan) Co., Ltd. FTIR spectra were recorded on an ATR spectrometer-733 (iN10MX). Raman spectra were recorded with a JY HR800 Raman spectrometer (HORIBA Jobin Yvon), equipped with a 50× objective (NA = 0.5) and a He–Ne laser with 633 nm wavelength, and a 785 nm excitation; the laser power values measured in the experiments were obtained from a power meter (15 mW at the samples with a spot area of approximately 1.4 μm^2). The Raman band of a silicon wafer at 520.8 cm^{-1} was used to calibrate the spectrometer. Finite difference time domain (FDTD) method was applied to visualize the EM enhancement distribution around the substrate. E-field distribution was calculated by numerically solving Maxwell's differential equations. Distance along three dimensions are divided into discrete segments as "Yee cell" while electric and magnetic fields are located on the edges and faces of the segments. Time is broken up into intervals. Electric and magnetic fields could be calculated alternately at the sequenced time and distance steps. The gold nanorod model was built as a column structure with a diameter of 20 nm and length of 60 nm, which was composited with two spherical ends at the bottom and top surface. Gold nanorod array model was designed according to SEM images. The excitation source with 633 nm wavelength was propagated along z-axis and polarized along y-axis or x-axis.

3. Results and Discussion

3.1. Mechanism

AuNRs/PMMA film as flexible SERS substrate was fabricated through self-assembly AuNRs in poly (methyl methacrylate) template, and the preparation procedure is shown in Scheme 1.

A thermodynamic model is always used to discuss aggregate states of spherical colloidal or nanorods at the oil–water interface [27–29]. However, unlike isotropic colloidal particles such as nanospheres, nanorods at interfaces show other distinctive responses due to their shape. The AuNRs oriented parallel rather than perpendicular to the water/toluene interface due to the former orientation can cover more surface and reduce more interfacial energies [27,30–32]. SEM image in Fig. 1(a) demonstrates a uniform and orderly arranged AuNRs array layer on the PMMA template, in which AuNRs are with a length of 62.7 ± 3.3 nm and the diameter of cross section is 21.7 ± 1.7 nm. When PMMA was added to toluene and contact with water, those hydrophobic molecules with a high dielectric constant will bound to oil-water interfaces because of image charge effects [33]. Hence, the PMMA move to the water/toluene interface as template to help AuNRs form orderly "hot spots" [34]. Elemental mapping within the supporting information Fig. S1 shows the homogeneous distribution of Au, C and O elements. Furthermore, the atomic percentages of Au, C and O are 25.23%, 64.39% and 10.38% respectively. These results clearly demonstrate the uniform distribution of AuNRs on the PMMA.

3.2. Optical Characterization

Fig. 1 (**b**) shows UV–vis spectra of monodispersed AuNRs solution (yellow line), those two strong plasmon peaks at 532 and 880 nm belong to transverse and longitudinal bands of the AuNRs. Pink line corresponds to UV–vis spectrum of AuNRs/PMMA film, in which the typical surface plasmon resonance (SPR) bands are broadened due to the assembly of AuNRs [35,36]. The blue line corresponds to UV–vis spectrum of AuNRs solution after assembly presents almost no SPR bands which means most of AuNRs particles have already rose up to PMMA template after reaction. FTIR spectra were also used to further analyze the formation of AuNRs/PMMA-PET film in Fig. S2. The bands at ca.1145 cm^{-1}, 1245 cm^{-1} and 1724 cm^{-1} are assigned to the C—O alkoxy stretching, C—O epoxy stretching and C═O carbonyl stretching vibrations,

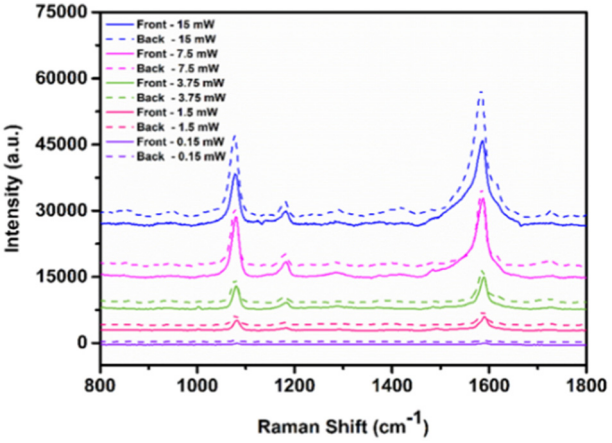

Fig. 2. SERS spectra measured from front (solid line) and back (dash line) sides of the AuNRs/PMMA film (10^{-3} M p-MBA as probe molecules) under different laser power. Laser wavelength is 633 nm and integration time is 5 s.

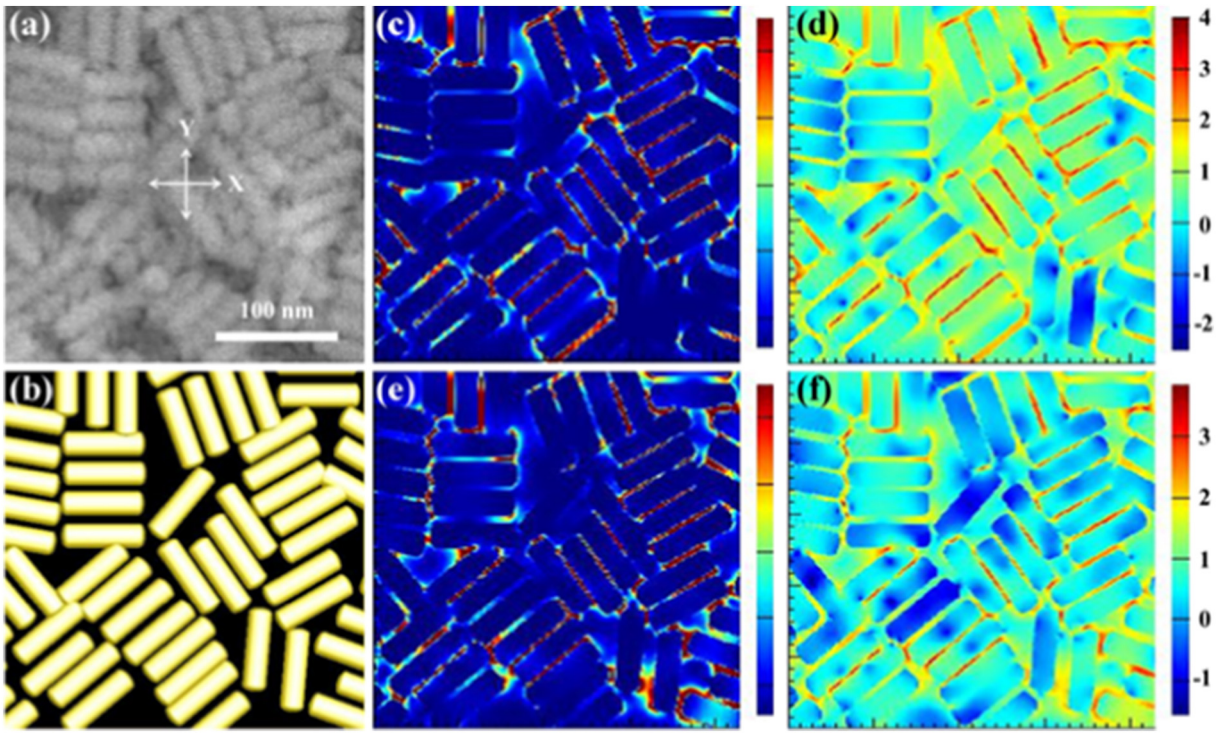

Fig. 3. 3D-FDTD model for Gold nanorod array (b) according to SEM images (a); 2D patterns of E-field intensity amplitude (|E|2) around the corresponding model with polarization along the x-axis (c–d) and y-axis (e–f). XY planes containing geometric centers of body structure were normal plotted with scale bar of 100 (c,e) and log-plotted (d,f).

respectively. It's worth to mention that the spectra of AuNRs/PMMA-PET film is similar to pure PMMA film but differed from pure PET film. This result indicates the PET as a support layer under the PMMA and barely influence the signal of the AuNRs/PMMA-PET film.

3.3. SERS Performance

Fig. 2 shows the SERS signals collected from both side of the AuNRs/PMMA-PET film under different laser power using 10^{-3} M p-MBA as analytes and 633 nm laser excitation. As PET and PMMA exhibit excellent optical transparency, the laser can easily pass through the PET and PMMA template and reach the assembled AuNRs layer. On this occasion, the Raman signal of analytes adsorbed on AuNRs layer will be amplified distinctly due to the greatly enhanced of the local electromagnetic field even the laser excited from the other side (PMMA side) of the film [37].

It should be pointed out that when the AuNRs/PMMA-PET film under high power laser (Fig. 2 blue line, 15 mW), SERS intensity of back side (PET) is stronger than the front side (AuNRs layer) which might be caused by the damage of the PMMA layer as well as the distortion of orderly arranged AuNRs layer. The Raman intensity tend to become identical when the laser power was turning down. Hence, we can obtain Raman signal from the side of PMMA while AuNRs layer connect with analytes. And realize high SERS performance as well as sample collection directly without destruction of the film structure while the laser power is about 7.5 mW. SERS spectra of AuNRs/PMMA film adsorbing different concentrations of pMBA standard samples from 10^{-4} M to 10^{-8} M was shown in Fig. S3 (a). And a control spectrum obtained from blank AuNRs/PMMA film was shown in Fig. S3 (b), there is little influence of blank AuNRs/PMMA film in SERS measurement.

To evaluate the SERS activity of the AuNRs/PMMA film, the Raman enhancement factor (EF) was calculated by employing the formula:

$$\mathbf{EF} = \frac{\boldsymbol{I_{SERS}}}{\boldsymbol{I_{bulk}}} \times \frac{\boldsymbol{N_{bulk}}}{\boldsymbol{N_{SERS}}}$$

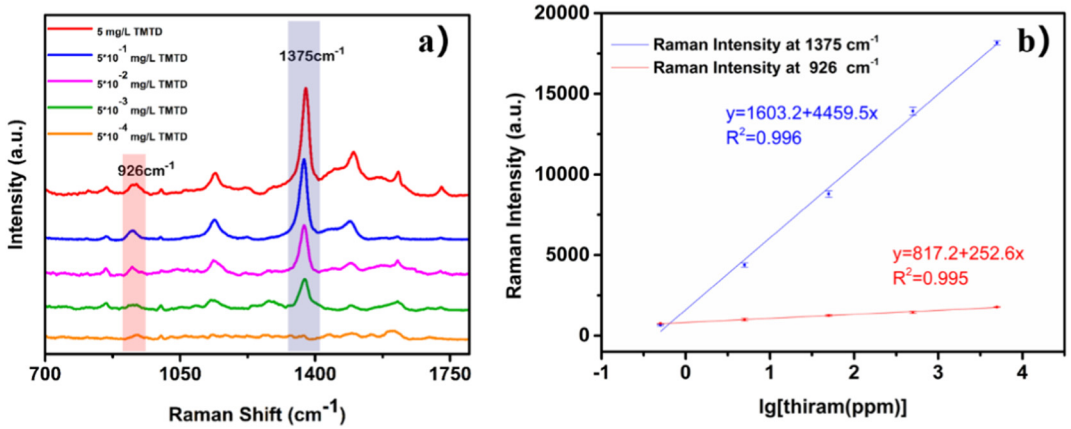

Fig. 4. (a) SERS spectra of AuNRs/PMMA film adsorbing different concentrations of thiram standard samples from 5 ppm to 0.5 ppb; (b) The Raman intensity at 926 cm^{-1} and 1380 cm^{-1} versus the logarithms of the thiram concentrations ranging from 5 ppm to 0.5 ppb.

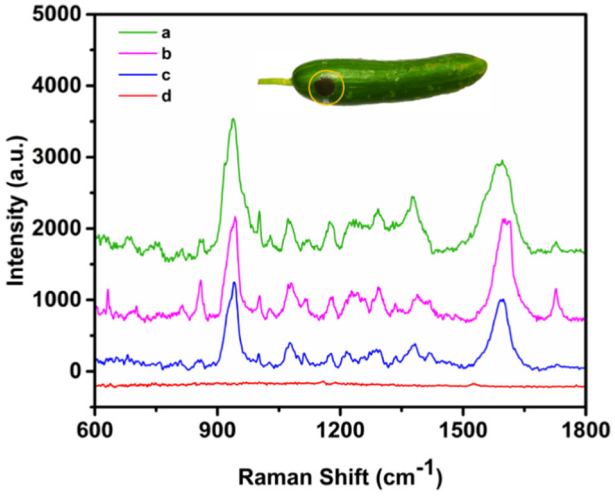

Fig. 5. SERS spectra of thiram (a:5 ppm; b:500 ppb; c:50 ppb) adsorbed on cucumber surface, acquired by wrapping the cucumber surface with AuNRs/PMMA film and the 785 nm laser is illuminating from the back side (PMMA side) of the film. The red line (d) was a control spectrum obtained from cucumber surface with 5 ppm thiram but without AuNRs/PMMA film. The inset shows a typical photograph of the detection on cucumber surface.

where I_{SERS} and N_{SERS} are normalized Raman peak intensities and the number of the reporter molecule chemisorbed on the SERS substrate; I_{NRS} and N_{NRS} are same parameters that in the reference solution. The calculation of N_{SERS} and N_{NRS} is relate to the area of the focal spot of the laser, the effective layer depth and the concentration of molecules [38]. The CV concentration is 10^{-9} M on the SERS substrate and 10^{-4} M in the reference solution. And the pMBA concentration is 10^{-8} M on the SERS substrate and 10^{-2} M in the reference solution. By substituting measured and calculated values into equation, the EF was calculated to be 1.6×10^5 according to peaks at 1620 cm^{-1} with CV as probe and was calculated to be 1.4×10^6 according to peaks at 1075 cm^{-1} with pMBA as probe, (Corresponding SERS spectra are provided in Supplementary data Fig. S4).

Finite difference time domain (FDTD) method was applied to visualize the EM enhancement distribution around the substrate. 3D-FDTD method was introduced to further understand the electromagnetic enhancement effect on the surface of substrates. E-field distribution was calculated by numerically solving Maxwell's differential equations. Distance along three dimensions are divided into discrete segments as "Yee cell" while electric and magnetic fields are located on the edges and faces of the segments. Time is broken up into intervals. Electric and magnetic fields could be calculated alternately at the sequenced time and distance steps. The gold nanorod model was built as a column structure with a diameter of 20 nm and length of 60 nm, which was composited with two spherical ends at the bottom and top surface. Gold nanorod array model was designed according to SEM images. The excitation source with 633 nm wavelength was propagated along z-axis and polarized along y-axis or x-axis as shown in Fig. 3. The refractive index of gold material is from Johnson and Christy data. The calculated electric field intensity ($|E|^2$) of the gold nanorod array model is shown in Fig. 3. Considering that the spectral enhancement in SERS varied as the fourth power of local field enhancement of substrates. The maximum enhancement factor ($|E|^4$) could reach a value of 10^8. In general, region with maximum enhancement accounts for less than 1% of the whole substrate surface, thus average enhancement could be approximately estimated to be 5–6 order of magnitudes, which agrees well with the experimental results.

The AuNRs/PMMA film was further applied for the detection of trace thiram, one of the dithiocarbamate compound that are widely used as insecticidal agents on food crops and vegetables [39]. SERS is considered as an effective method for rapid detection of trace thiram due to the existence of S—S bond which can easily forms a resonated radical structure while interacting with Au surface [40]. Fig. 4 (**a**) shows the Raman spectra of thiram standard samples with concentrations of 5 ppm, 500 ppb, 50 ppb, 5 ppb and 0.5 ppb, using the AuNRs/PMMA film as SERS substrate. The characteristic peak of thiram at 926 cm^{-1} is attributed to the stretching CH_3N and C═S vibration modes, 1138 cm^{-1} and 1500 cm^{-1} belong to CN stretching vibrations and rocking CH_3 mode, and the peak of 1375 cm^{-1} is assigned to the CN stretching mode and symmetric CH_3 deformation mode [41]. It can be seen that the lowest detection concentration of thiram is 0.5 ppb, which is lower than the maximal residue limit of 5 ppm in fruit prescribed by the GB. Furthermore, in Fig. 4 (**b**) a good direct proportionality was obtained between the SERS intensity at 1380 cm^{-1} and the logarithms of thiram concentrations in the range of 5 ppm to 0.5 ppb, which satisfied the linear relationship of $y = 1857.4 + 4406.4\times$ with a squared correlation coefficient (R^2) of 0.998, and another calibration curve for peak at 926 cm^{-1} satisfied the linear relationship of $y = 822.5 + 256.6\times$ with a squared correlation coefficient (R^2) of 0.999.

3.4. Application as Flexible SERS Substrate

Prior to probing the analyte, we recorded the direct sampling and detection of thiram on cucumber surface under 785 nm laser excitation (7.5 mW). First, pieces of cucumber were soaked in thiram solutions with different concentrations (from 5 ppm to 50 ppb), then covered an AuNRs/PMMA film around the surface with the AuNRs facing it for pesticide detection. As shown in Fig. 5, the recoveries (the details were shown in supplementary data) of three different concentration standard addition are 106.3%, 98.4% and 94.2% corresponding to

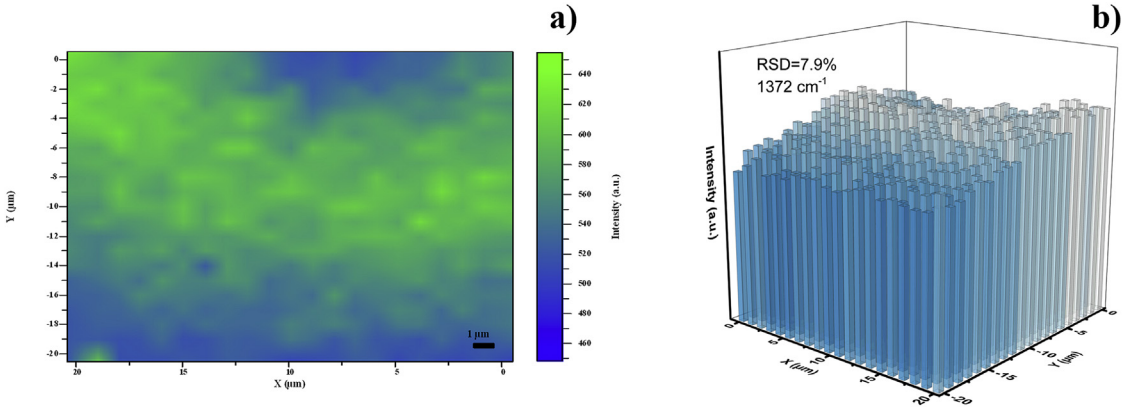

Fig. 6. (a) Raman intensity maps at 1372 cm^{-1} of 0.5 ppm thiram molecules on a 20×20 μm2 surface area of the AuNRs/PMMA film. Laser wavelength is 785 nm, power is 3.25 mW and integration time is 1 s; (b) The corresponding intensity distributions at 1372 cm^{-1} of thiram molecules in (a).

5 ppm, 500 ppb and 50 ppb, the good recoveries indicate the AuNRs/PMMA film has great potential of realistic application.

3.5. SERS Reproducibility of the AuNRs/PMMA Film

In order to investigate the homogeneity and stability of the AuNRs/PMMA flexible substrate, we employ a SERS mapping measurement via spot to spot Raman spectra on a $20 \times 20\ \mu m^2$ area of 0.5 ppm thiram absorbed on AuNRs/PMMA film with a step size of 1 μm to evaluate the substrate reproducibility. As shown in Fig. 6, the relative standard deviation (RSD) was calculated to be 7.9% for Raman intensity at 1372 cm^{-1}, indicating good uniformity in large area. This result proves that the AuNRs/PMMA film can be used as a SERS substrate with high reproducibility due to uniform AuNRs array.

4. Conclusions

In summary, we adopted a rapid and effective method to fabricate the AuNRs/PMMA film served as a flexible SERS substrate. This film offers great flexibility, high SERS activity and excellent optical transparency. The PMMA process as a template to help AuNRs packing orderly. The AuNRs/PMMA film could be used as SERS substrate with a high EF of 1.6×10^5 due to the "hot spots" between different AuNRs in the array. The lowest detection concentration of thiram could reach a value of 0.5 ppb, and quantitative analysis was also achieved in the range of 5 ppm–0.5 ppb. The AuNRs/PMMA film also facilitates direct SERS detection of trace thiram on cucumber surface with a satisfactory. Thus, this AuNRs/PMMA flexible substrate is expected to exhibit great potential for applications in realistic detection.

Acknowledgments

This work was supported by the National Natural Science Foundation of China (51572009). Authors have nothing to disclose.

Appendix A. Supplementary data

Supplementary data to this article can be found online at https://doi.org/10.1016/j.saa.2018.05.068.

References

[1] N.P. Pieczonka, R.F. Aroca, Single molecule analysis by surfaced-enhanced Raman scattering, Chem. Soc. Rev. 37 (2008) 946–954.
[2] M. Fan, G.F.S. Andrade, A.G. Brolo, A review on the fabrication of substrates for surface enhanced Raman spectroscopy and their applications in analytical chemistry, Anal. Chim. Acta 693 (2011) 7–25.
[3] M. Cueto, M. Piedrahita, C. Caro, B. Martinez-Haya, M. Sanz, M. Oujja, M. Castillejo, Platinum nanoparticles as photoactive substrates for mass spectrometry and spectroscopy sensors, J. Phys. Chem. C 118 (2014) 11432–11439.
[4] C. Caro, M.J. Sayagues, V. Franco, A. Conde, P. Zaderenko, F. Gamez, A hybrid silver-magnetite detector based on surface enhanced Raman scattering for differentiating organic compounds, Sens. Actuators, B 228 (2016) 124–133.
[5] M.J. Natan, Surface Enhanced Raman Scattering, Plenum Pr, 1982.
[6] M. Moskovits, M. Moskovits, Surface-enhanced Raman spectroscopy: a brief retrospective, J. Raman Spectrosc. 36 (2005) 485–496.
[7] P.L. Stiles, J.A. Dieringer, N.C. Shah, R.R. Van Duyne, Surface-enhanced Raman spectroscopy, Annu. Rev. Anal. Chem. 1 (2008) 601–626.
[8] J.F. Li, Y.F. Huang, Y. Ding, Z.L. Yang, S.B. Li, X.S. Zhou, F.R. Fan, W. Zhang, Z.Y. Zhou, Y. Wu de, B. Ren, Z.L. Wang, Z.Q. Tian, Shell-isolated nanoparticle-enhanced Raman spectroscopy, Nature 464 (2010) 392–395.
[9] K. Kneipp, H. Kneipp, I. Itzkan, R.R. Dasari, M.S. Feld, TOPICAL REVIEW: surface-enhanced Raman scattering and biophysics, J. Phys. Condens. Matter 14 (2002) R597–R624.
[10] E.C.L. Ru, P.G. Etchegoin, Recent developments - principles of surface-enhanced Raman spectroscopy - chapter 8, Principles of Surface-Enhanced Raman Spectroscopy, 47, 2009, pp. 415–464.
[11] V.P. Menon, C.R. Martin, Fabrication and evaluation of nanoelectrode ensembles, Anal. Chem. 67 (1995) 1920–1928.
[12] N. Marquestaut, A. Martin, D. Talaga, L. Servant, S. Ravaine, S. Reculusa, D.M. Bassani, E. Gillies, F. Lagugnélabarthet, Raman enhancement of azobenzene monolayers on substrates prepared by Langmuir-Blodgett deposition and electron-beam lithography techniques, Langmuir 24 (2008) 11313–11321.
[13] L. Polavarapu, L.M. Liz-Marzán, Towards low-cost flexible substrates for nanoplasmonic sensing, Phys. Chem. Chem. Phys. 15 (2013) 5288–5300.
[14] J.P. Singh, H. Chu, J. Abell, R.A. Tripp, Y. Zhao, Flexible and mechanical strain resistant large area SERS active substrates, Nano 4 (2012) 3410–3414.
[15] Y. Qian, G. Meng, Q. Huang, C. Zhu, Z. Huang, K. Sun, B. Chen, Flexible membranes of Ag-nanosheet-grafted polyamide-nanofibers as effective 3D SERS substrates, Nano 6 (2014) 4781–4788.
[16] J. K., B. S., M. Ganiga, M. Ganiga, B.K. George, Effective SERS detection using a flexible wiping substrate based on electrospun polystyrene nanofibers, Anal. Methods 9 (2017) 3998–4003.
[17] W. Xin, J.M. Yang, C. Li, M.S. Goorsky, L. Carlson, I.D. Rosa, A novel strategy for one-pot synthesis of gold nanoplates on carbon nanotube sheet as an effective flexible SERS substrate, ACS Appl. Mater. Interfaces 9 (2017) 6246–6254.
[18] M. Yilmaz, M. Erkartal, M. Ozdemir, U. Sen, H. Usta, G. Demirel, Three dimensional Au-coated electrosprayed nanostructured BODIPY films on aluminum foil as surface-enhanced Raman scattering platforms and their catalytic applications, ACS Appl. Mater. Interfaces 9 (2017) 18199–18206.
[19] A. Lamberti, A. Virga, A. Angelini, A. Ricci, E. Descrovi, M. Cocuzza, F. Giorgis, Metal-elastomer nanostructures for tunable SERS and easy microfluidic integration, RSC Adv. 5 (2014) 4404–4410.
[20] L.B. Zhong, J. Yin, Y.M. Zheng, Q. Liu, X.X. Cheng, F.H. Luo, Self-assembly of Au nanoparticles on PMMA template as flexible, transparent, and highly active SERS substrates, Anal. Chem. 86 (2014) 6262–6267.
[21] L. Z, M. G, H. Q, H. X, H. X, T. H, W. Z, L. F, Ag nanoparticle-grafted PAN-nanohump array films with 3D high-density hot spots as flexible and reliable SERS substrates, Small 11 (2015) 5452–5459.
[22] H. Xu, J. Aizpurua, M. Kall, P. Apell, Electromagnetic contributions to single-molecule sensitivity in surface-enhanced raman scattering, Phys. Rev. E Stat. Phys. Plasmas Fluids Relat. Interdiscip. Topics 62 (2000) 4318.
[23] J. Gersten, A. Nitzan, Electromagnetic theory of enhanced Raman scattering by molecules adsorbed on rough surfaces, J. Chem. Phys. 73 (1980) 3023–3037.
[24] M. Moskovits, Surface-enhanced spectroscopy, Rev. Mod. Phys. 57 (1985) 783–826.
[25] N. Yang, T.T. You, X. Liang, C.M. Zhang, L. Jiang, P.G. Yin, An ultrasensitive near-infrared satellite SERS sensor: DNA self-assembled gold nanorod/nanospheres structure, RSC Adv. (2017) 9321–9327.
[26] X. Ye, Z. Chen, J. Chen, Y. Gao, C.B. Murray, Using binary surfactant mixtures to simultaneously improve dimensional tunability and monodispersity in the seeded-growth of gold nanorods, Nano Lett. 13 (2013) 765–771.
[27] S. Kutuzov, J. He, R. Tangirala, T. Emrick, T.P. Russell, A. Böker, On the kinetics of nanoparticle self-assembly at liquid/liquid interfaces, Phys. Chem. Chem. Phys. 9 (2007) 6351–6358.
[28] N. Z, H. J, R. TP, W. Q, Synthesis of nano/microstructures at fluid interfaces, Angew. Chem. 49 (2010) 10052–10066.
[29] L. Hu, M. Chen, X. Fang, L. Wu, Oil-water interfacial self-assembly: a novel strategy for nanofilm and nanodevice fabrication, Chem. Soc. Rev. 43 (2012) 1350–1362.
[30] L. Dong, D.T. Johnson, Adsorption of acicular particles at liquid-fluid interfaces and the influence of the line tension, Langmuir 21 (2005) 3838–3849.
[31] J. He, Q. Zhang, S. Gupta, T. Emrick, T.P. Russell, P. Thiyagarajan, Drying droplets: a window into the behavior of nanorods at interfaces, Small 3 (2007) 1214–1217.
[32] J. He, Z. Niu, R. Tangirala, J.Y. Wang, X. Wei, G. Kaur, Q. Wang, G. Jutz, A. Böker, B. Lee, Self-assembly of tobacco mosaic virus at oil/water interfaces, Langmuir 25 (2009) 4979–4987.
[33] M.E. Leunissen, A.V. Blaaderen, A.D. Hollingsworth, M.T. Sullivan, P.M. Chaikin, Electrostatics at the oil-water interface, stability, and order in emulsions and colloids, Proc. Natl. Acad. Sci. U. S. A. 104 (2007) 2585–2590.
[34] C.N.R. Rao, K.P. Kalyanikutty, The liquid–liquid Interface as a medium to generate nanocrystalline films of inorganic materials, Acc. Chem. Res. 41 (2008) 489–499.
[35] L. Tian, Q. Jiang, K.K. Liu, J. Luan, R.R. Naik, S. Singamaneni, Nanocellulose films: bacterial nanocellulose-based flexible surface enhanced raman scattering substrate (Adv. Mater. Interfaces 15/2016), Adv. Mater. Interfaces 3 (2016) n/a-n/a.
[36] B. Peng, G.Y. Li, D.H. Li, S. Dodson, Q. Zhang, J. Zhang, Y.H. Lee, H.V. Demir, X.Y. Ling, Q.H. Xiong, Vertically aligned gold nanorod monolayer on arbitrary substrates: self-assembly and femtomolar detection of food contaminants, ACS Nano 7 (2013) 5993–6000.
[37] C. Chen, J.A. Hutchison, F. Clemente, R. Kox, H. Ujii, J. Hofkens, L. Lagae, G. Maes, G. Borghs, D.P. Van, Direct evidence of high spatial localization of hot spots in surface-enhanced Raman scattering, Angew. Chem. 121 (2009) 10116–10119.
[38] H.Y. Jia, J.B. Zeng, W. Song, J. An, B. Zhao, Preparation of silver nanoparticles by photo-reduction for surface-enhanced Raman scattering, Thin Solid Films 496 (2006) 281–287.
[39] V.K. Sharma, J.S. Aulakh, A.K. Malik, Thiram: degradation, applications and analytical methods, J. Environ. Monit. 5 (2003) 717.
[40] X. Liang, Y.S. Wang, T.T. You, X.J. Zhang, N. Yang, G.S. Wang, P.G. Yin, Interfacial synthesis of a three-dimensional hierarchical MoS2-NS@Ag-NP nanocomposite as a SERS nanosensor for ultrasensitive thiram detection, Nano 9 (2017) 8879–8888.
[41] B. Liu, G. Han, Z. Zhang, R. Liu, C. Jiang, S. Wang, M.Y. Han, Shell thickness-dependent Raman enhancement for rapid identification and detection of pesticide residues at fruit peels, Anal. Chem. 84 (2012) 255–261.